Van Wyk de Vries, M. et al., 2022, Atypical landslide induces speedup, advance, and long-term slowdown of a tidewater glacier: Geology, v. 50, https://doi.org/10.1130/G49854.1

Supplement to: *Atypical landslide induces speedup, advance, and long-term slowdown of a tidewater glacier*

Maximillian Van Wyk de Vries[1,2], Andrew D. Wickert[1,2], Kelly R. MacGregor[3], and Camilo Rada[4], and Michael J. Willis[5]

Table of contents:

Section S1) Long-term ice loss

We do not evaluate causal links between glacial retreat and slope instability in this paper. Nevertheless, it is useful to note that several hundred metres of ice thinning have occurred all around Reclus over the past century, exposing a large area of steep, unconsolidated slope. Amalia's calving front has also retreated almost 10 km over the same period.

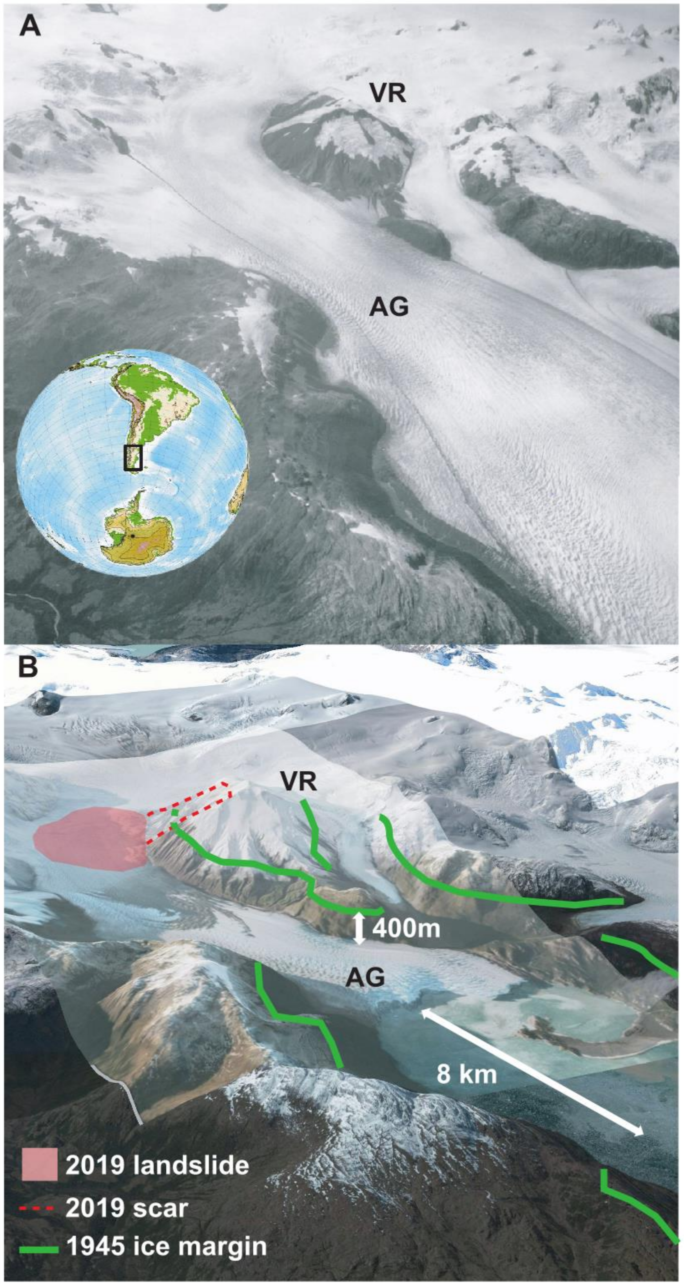

Figure S1: Location of Amalia Glacier (AG), Volcán Reclus (VR) and glacier retreat over the past 75 years. (A) Aerial photograph of AG from the 1944–1945 USAF Trimetrogon survey of Chile. (B) Sentinel 2 and Google Earth satellite imagery of AG from 02/2020. The 26/04/2019 landslide deposit is highlighted in red, and the 2017 landslide is also visible in the foreground.

Section S2) Landslide structure

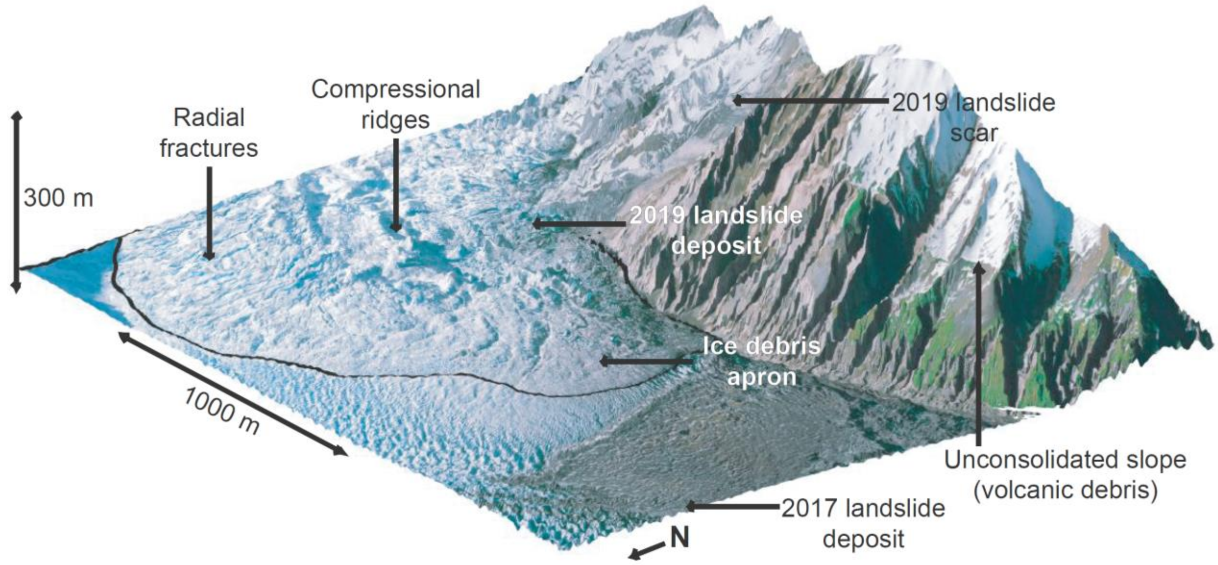

Figure S2: Annotated DigitalGlobe image of the Amalia glacier landslide, taken on 23 August 2019. The imagery is draped over a DEM of the same date. Note the substantial debris visible in the 2017 landslide deposit and close to no debris visible atop the ice from the 2019 landslide event, despite the latter being an order of magnitude larger.

Section S3) Landslide volume calculation

2017 Landslide

We calculate the volume of the earlier 2017 landslide by differencing a pre-event DEM (2011 TanDEM-X digital elevation model) and post- event DEM (derived from DigitalGlobe imagery). The volume of the scar is 18.3 million m^3, or 18.3±3.7 million m^3 accounting for 20% uncertainty in the measurement.

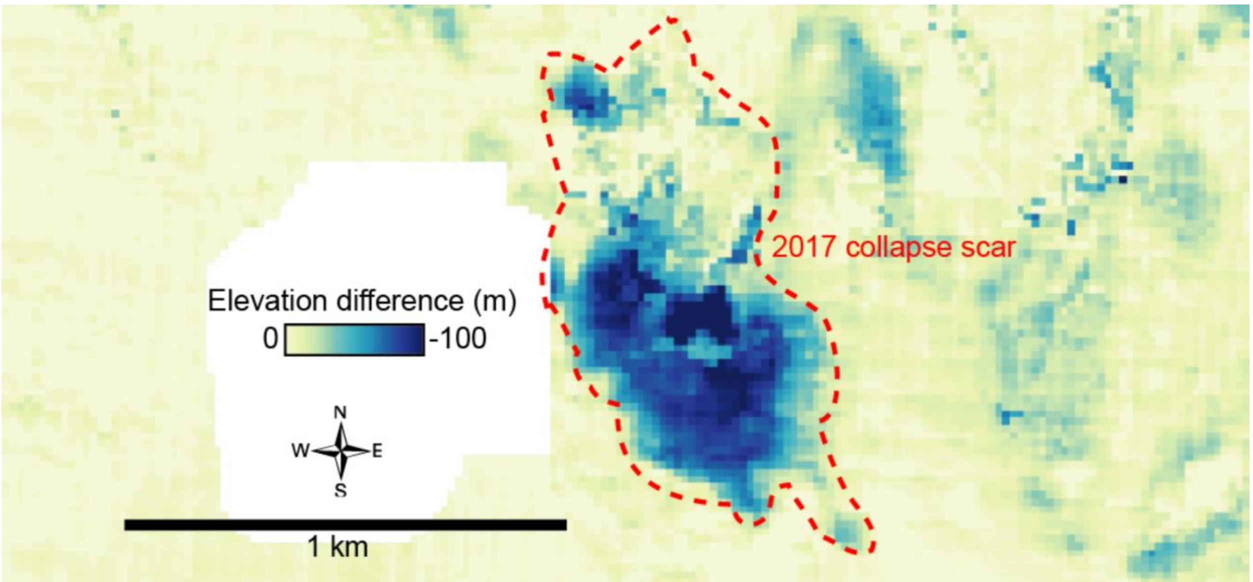

Figure S3: 2017 landslide collapse scar and DEM difference map.

2019 Landslide

We calculate the volume of the 2019 Reclus/Amalia landslide based on differencing of pre- and post-event 2m resolution DEMs over the landslide scar. Our pre-event DEM is from 28 May 2017, and the post-event DEM is from 23 August 2019. The 2-m-resolution DEMs were generated by applying stereo autocorrelation to overlapping pairs of high-resolution DigitalGlobe satellite imagery. Analysis of Sentinel-2 optical satellite imagery between these dates shows that no other major landslides have occurred, and that any elevation change is a consequence of the 26 April 2019 landslide discussed in this paper.

Portions of the slope are absent from the post-event DEM, and we manually infill these to match the scar extent visible in Sentinel-2 imagery using a DEM editor (Surfer 16™). We assign a conservative 50% uncertainty to manually interpolated portions of the collapse scar, and 20% uncertainty to areas with data coverage. The result of this is shown in Supplementary Figure 2 below. Our data covers around two-thirds of the collapse area, which has a volume of 181±36 million m^3. The remaining portion of the scar has a volume of 81±41 million m^3, for a total landslide volume of 262±77 million m^3.

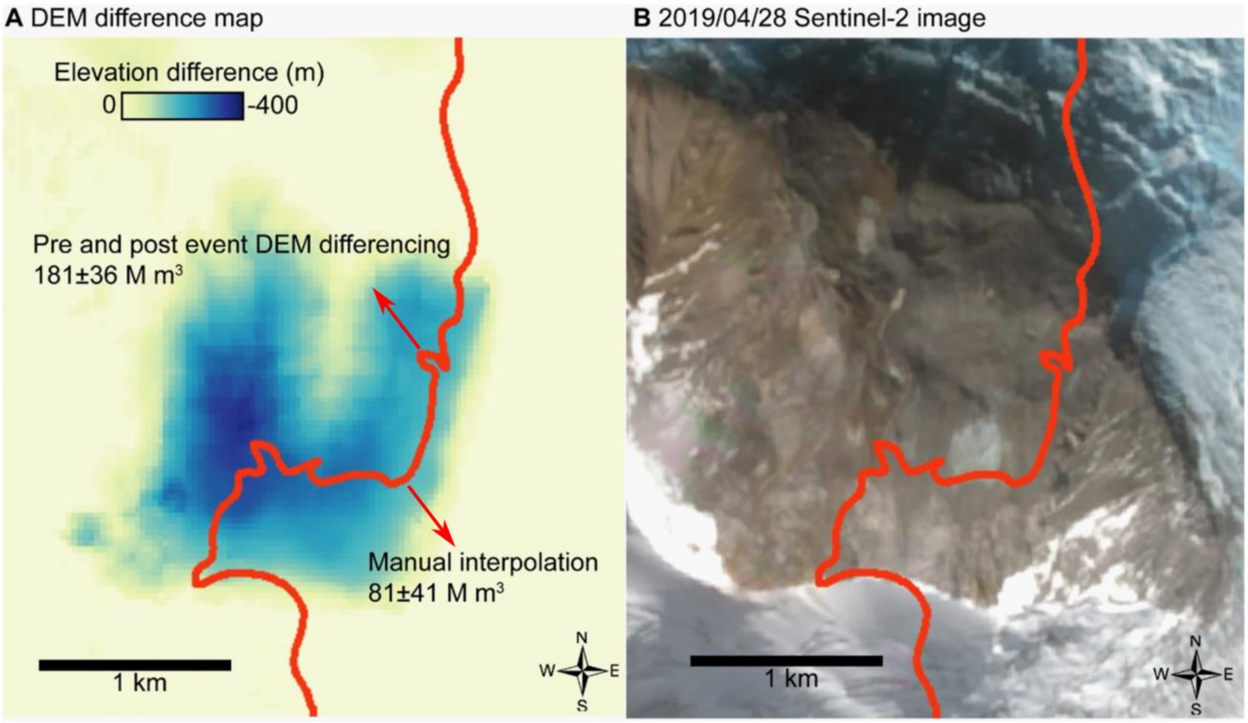

Figure S4: Landslide volume calculation. **A** shows the post- minus pre-event DEM difference map. **B** shows a post-event satellite image of the collapse scar.

Section S4) ISSM synthetic glacier model

We run a synthetic glacier model using the Ice Sheet and Sea Level System Model (ISSM; Larour et al., 2012; Morlighem et al., 2013). We input synthetic glacier-surface topography and ice thickness (approximately equivalent to that observed at Amalia: Carrivick et al., 2016; Millan et al., 2019), and manually calibrate a constant basal friction coefficient such that surface velocities are on the same order as those observed at Amalia.

We use a 100-m grid resolution and build our initial synthetic glacier geometry according to the following rules:

- Glacier surface topography is constant in the transverse direction and slopes 3.5 degrees in the longitudinal direction.
- Glacier thickness is constant in the longitudinal direction, and varies between 10 and 400 metres in the transverse direction defined by the following equation: Thickness = 10+400-abs(100*[distance across profile]-1550)^2*400/210.25
- Our model domain is 3 km wide and 10 km long, buffered on the upstream and downstream ends with an additional 5 km in order to avoid boundary effects.
- The subglacial landslide emplacement is simplified to a half-cone with a radius of 1400 m and height 250 m, for a total volume of 257 million cubic metres. The landslide is emplaced at the margin of the glacier, 6 km upglacier from the model front (excluding downglacier buffer).

We use a three-dimensional model setup with higher-order field equations (Blatter, 1995; Pattyn, 2003), the full derivation of which is provided in the ISSM documentation (https://issm.jpl.nasa.gov/documentation/stressbalance/). A schematic of the model geometry is provided in figure S5 below.

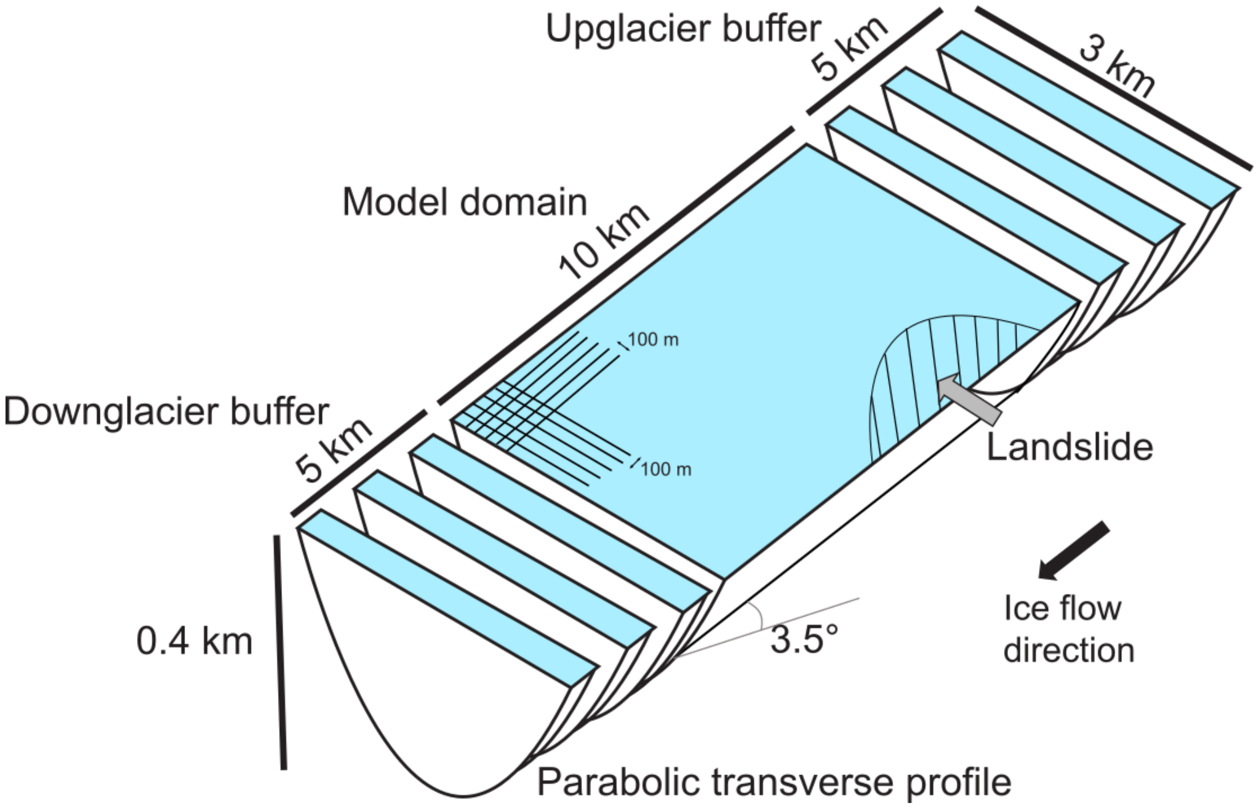

Figure S5: ISSM synthetic glacier model setup

We bring the modelled glacier to an initial steady-state geometry and velocity field by spinning it up for 10 years, using a timestep of 0.1 yr. We then use the final stage of this spin-up to initialize five different cases – each run for 5 years with a timestep of 0.01 year:

- Case 1: No landslide emplacement and no change in basal friction coefficient.
- Case 2: No landslide emplacement and a 20% decrease in basal friction coefficient.
- Case 3: No landslide emplacement and a 20% increase in basal friction coefficient.
- Case 4: Landslide emplacement and no change in basal friction coefficient.
- Case 5: Landslide emplacement and a 20% decrease in basal friction coefficient.
- Case 6: Landslide emplacement and a 20% increase in basal friction coefficient.

The full code used to run the ISSM model runs, and associated output files are provided in the following Zenodo repository: 10.5281/zenodo.5638870.

Section S5) Amalia glacier pre-landslide seasonal velocity cycle

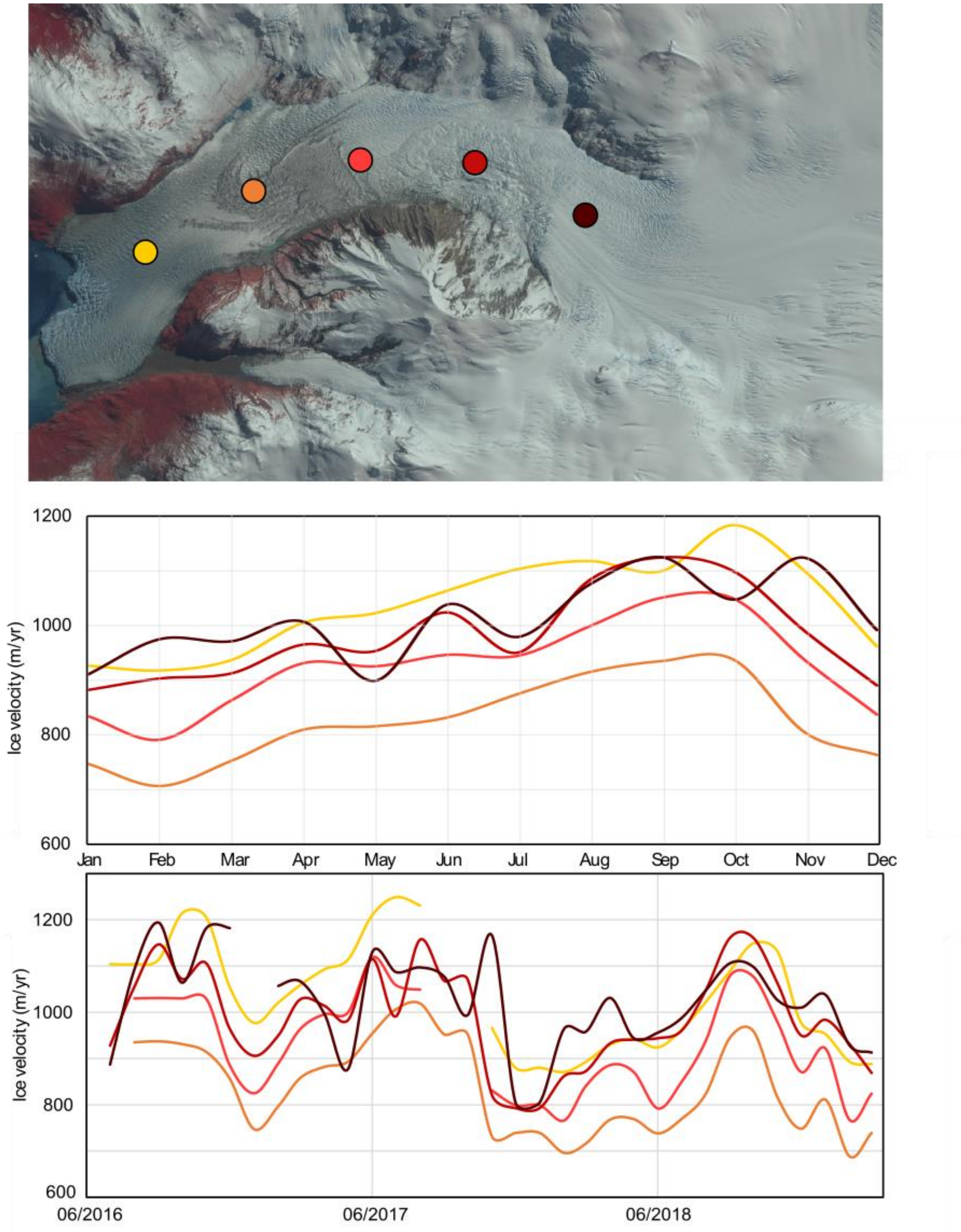

Figure S6: Pre-landslide seasonal ice speed cycle at different points on Amalia glacier. The seasonal variability is between 10 and 20% of the mean velocity, with a maximum in early S. hemisphere spring (Aug-Oct) and a minimum in late S. hemisphere summer (Jan-Mar). Averages are calculated using all available data within the period between January 2016 and March 2019 (inclusive). Raw down-glacier velocities are also given in Supplementary Table 1.

Table S1: Seasonal ice speed cycle at Amalia glacier. The first two rows provide the latitude and longitude of the points used (see also Figure S6), the following 12 rows provide the pre-landslide monthly-averaged velocities at each of these points, and the final row provides the overall pre-landslide velocity measured at each point.

Lat	**-50.9295**	**-50.9212**	**-50.9158**	**-50.9184**	**-50.9284**
Long	**-73.6529**	**-73.6311**	**-73.6111**	**-73.5683**	**-73.5465**
Jan	936.6667	765.6667	848.6667	894.3333	921.5
Feb	928.3333	727	807.6667	914.3333	983
Mar	946.6667	771	876.3333	923.3333	979.3333
Apr	1011.5	825	941	973.5	1013.5
May	1028	831	935.5	962	910.5
Jun	1067	846	955.5	1029.5	1043
Jul	1105	887.5	954	959.6667	987
Aug	1119	925.6667	1005.667	1086.333	1078.667
Sep	1101.5	944.6667	1055	1125.333	1125.667
Oct	1181.5	947.3333	1053.5	1101.333	1052
Nov	1100.667	820	946	996.3333	1124.667
Dec	970.3333	781	851.6667	902.3333	999
Mean	1041.347	839.3194	935.875	989.0278	1018.153

Section S6) 2021 glacier change

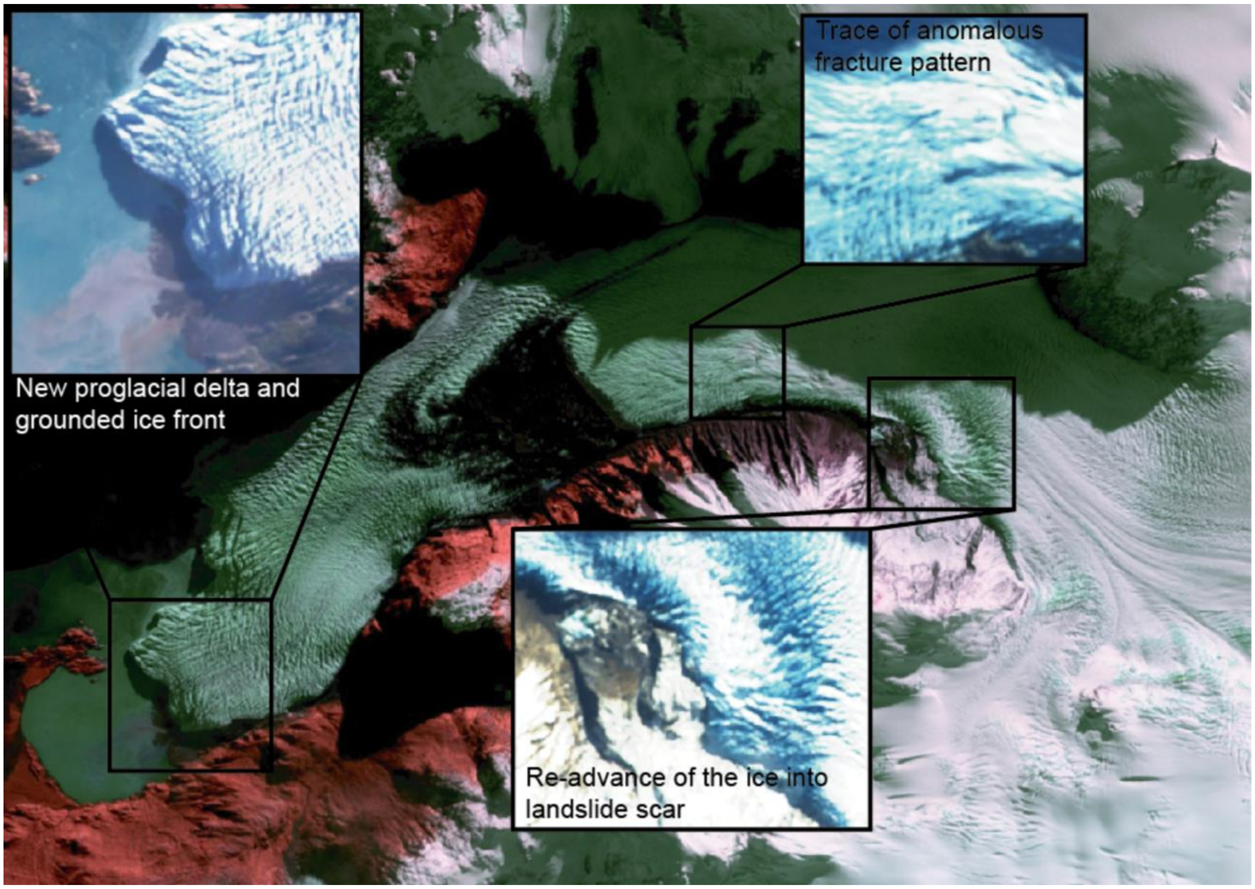

Figure S7: 7 May 2021 false color Sentinel-2 Image of Amalia glacier showing key zones of the glacier. Note again the complete absence of visible debris in the 2019 landslide impact zone, relative to the smaller 2017 event. The insets are given in true color.

Section S7) Suspended sediment calculations

We modify the Ulysses Water Quality Viewer (Zlinszky and Padányi-Gulyás, 2020) in order to remove all non-water bodies calculate relative suspended-sediment concentrations (SSCs) in water areas. Figure S8 below shows an example of the resulting maps: light colors have low relative SSC, brown colored areas have high relative SSC and non-water areas are masked out (black).

We filter each 10m resolution Sentinel-2 relative SSC image to exclude high-wavenumber noise – typically from icebergs – while retaining the lower-wavenumber signal from sediment plumes. We remove pixels that differ more than 50% from the mean of the 4 neighboring pixels and more than 100% from the 49-point mean (using a 7 by 7 diamond shaped kernel centered on the pixel). We then calculate the mean relative SSC values of all remaining pixels over the first five kilometers from Amalia's calving front to identify periods of anomalously high sediment output.

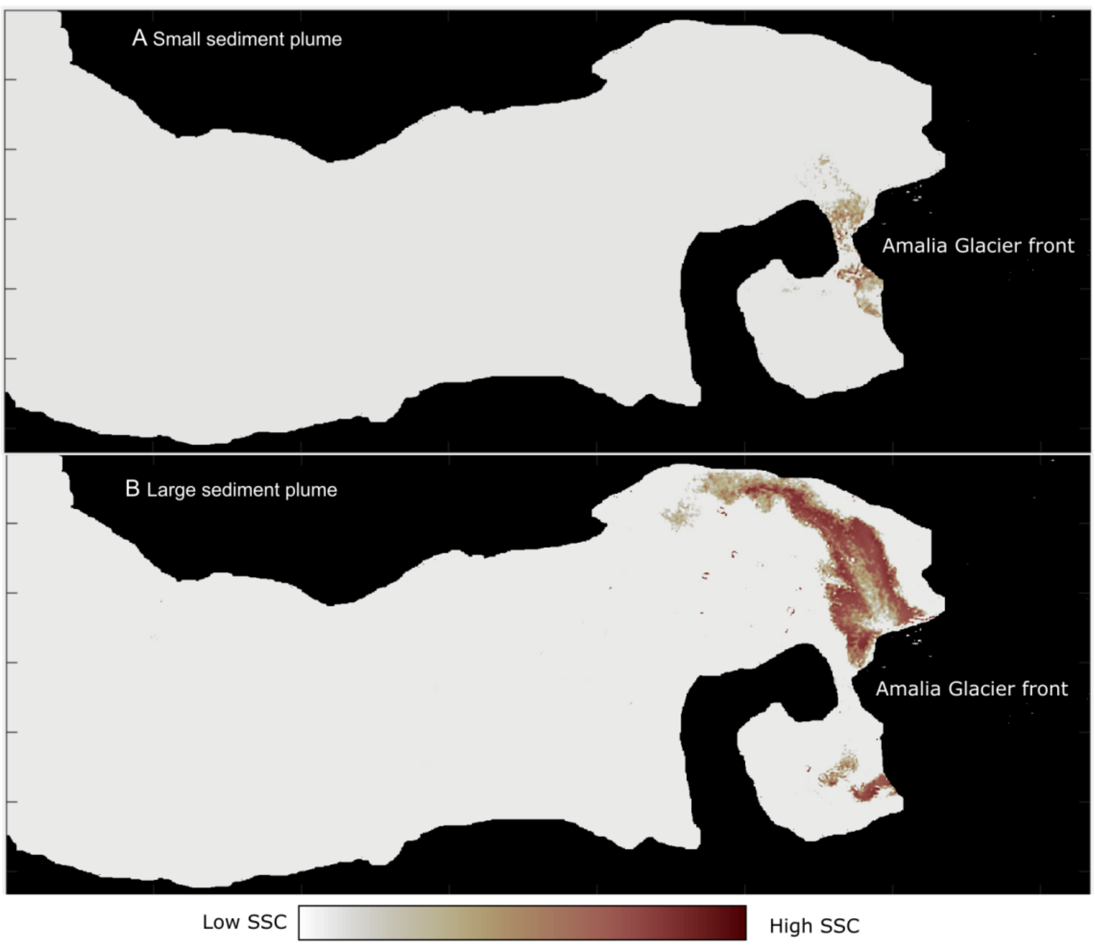

Figure S8: Example of a small and large sediment plume in Amalia fjord, used as inputs for the filtering step described above. Black areas were masked out.

Section S8) Comparison with external glacier velocity dataset

We compare our Sentinel-2-derived glacier-velocity dataset with an externally derived dataset calculated using Sentinel-1 radar (Friedl et al., 2021). The Sentinel-1 data have a lower spatial resolution (200 m), and the same temporal resolution (1 month) as our data. The two datasets show the same pattern of velocity change over time, with an initial bimodal change (acceleration downglacier, deceleration upglacier) and a longer term widespread slowdown. Both remotely sensed velocity fields demonstrate continued slowdown at the ice front 2 years following the landslide, but return to within 10% of pre-landslide ice speeds at the landslide emplacement zone.

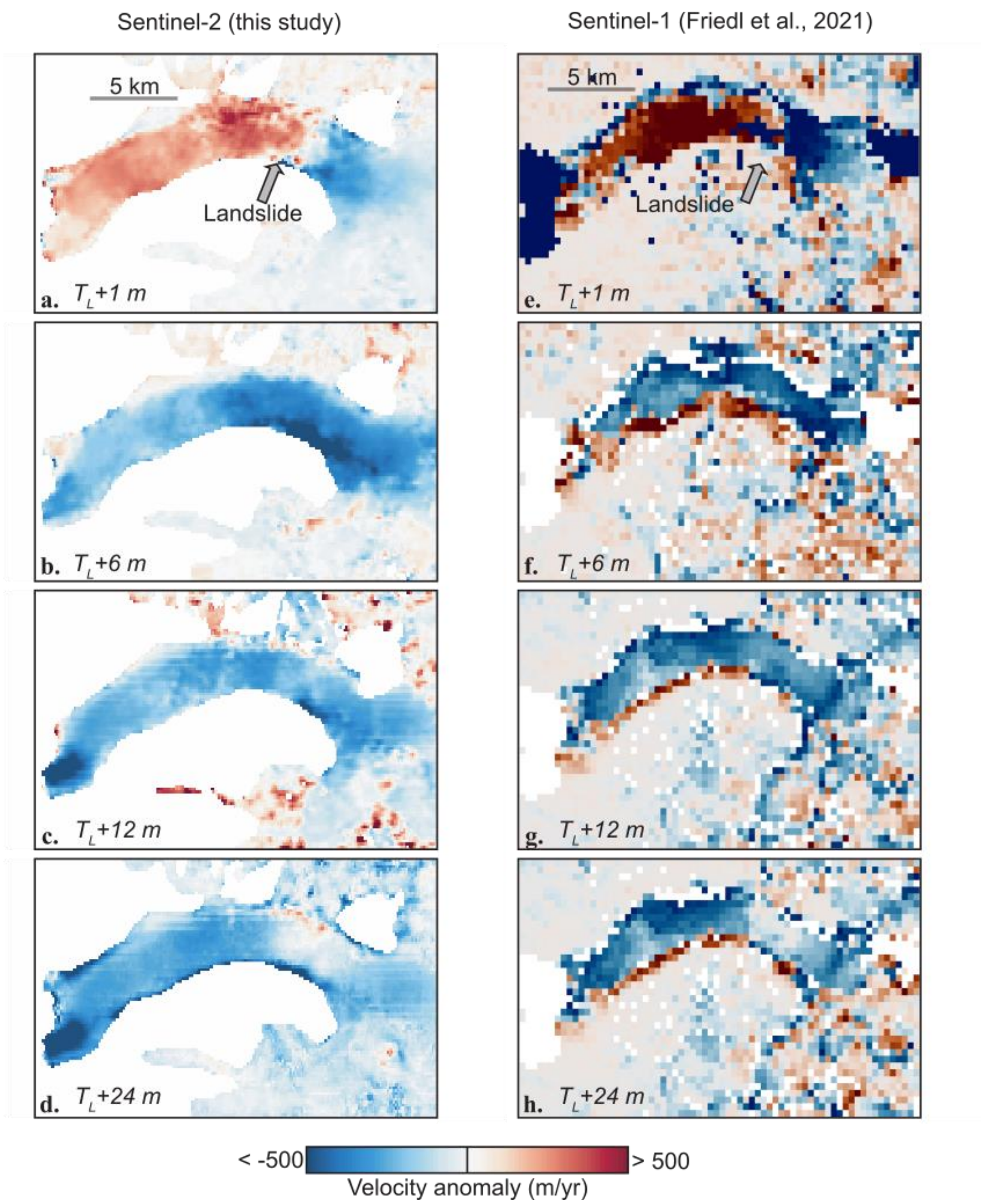

Figure S9: Comparison of optical-feature-tracking speeds derived from this study (a-d) with radar speckle tracking results from Friedl et al., 2021 (e-h).

Section S9) List of Sentinel-2 images used in feature tracking

Table S2: Full date list (yyyymmdd format) of the Sentinel-2 images used in glacier surface velocity calculations.

20151001	20171104	20180717	20181212	20190710	20200417	20210209
20160518	20171109	20180725	20190108	20190712	20200425	20210216
20160710	20171129	20180727	20190116	20190715	20200427	20210226
20160717	20180205	20180801	20190123	20190717	20200505	20210301
20160730	20180217	20180806	20190126	20190811	20200611	20210303
20160806	20180227	20180809	20190205	20190814	20200614	20210328
20160826	20180304	20180816	20190227	20190816	20200616	20210331
20160928	20180324	20180819	20190312	20190819	20200626	20210405
20161018	20180327	20180824	20190314	20190905	20200629	20210420
20161204	20180329	20180831	20190411	20190925	20200704	20210507
20170222	20180413	20180905	20190423	20190928	20200706	20210510
20170327	20180501	20180908	20190428	20190930	20200716	20210515
20170403	20180506	20180910	20190503	20191008	20200719	20210517
20170416	20180513	20180920	20190506	20191013	20200825	20210522
20170526	20180516	20180923	20190508	20191015	20200904	20210604
20170602	20180528	20180925	20190528	20191030	20200907	20210616
20170615	20180602	20180930	20190531	20191109	20200909	
20170630	20180610	20181008	20190602	20200101	20201002	
20170707	20180612	20181018	20190612	20200202	20201101	
20170712	20180627	20181023	20190615	20200207	20201106	
20170727	20180702	20181025	20190617	20200210	20201228	
20170809	20180705	20181030	20190627	20200220	20210115	
20170923	20180710	20181102	20190702	20200222	20210125	
20171102	20180715	20181127	20190707	20200306	20210206	

Section S10) Data normalizations

In figure 2 (main manuscript), glacier-surface velocity, relative SSCs, calving flux, and frontal position are all provided relative to pre-landslide values.

Glacier-surface velocity is normalized relative to mean pre-landslide velocities. To account for any seasonal variability, we create a second normalization for each month. Normalized glacier surface velocity u_N is thus given by:

$$u_N = \frac{u_i}{\tilde{u}_i}$$

With u_i velocity for a given month i and $\tilde{u}_i$ pre-landslide (2016-2019) mean velocity for a given month i.

Relative suspended-sediment concentration is further normalized to the pre-landslide average (2016-2019) relative suspended-sediment concentration values (calculated as described in section S7), as is the calving flux.

Normalized rSSC (ssc_N) and calving flux (c_N) are given by

$$ssc_N = \frac{ssc}{\widetilde{ssc}}$$

And

$$c_N = \frac{c}{\tilde{c}}$$

With ssc and c being individual calving flux and suspended sediment concentration calculations, and $\widetilde{ssc}$ and $\tilde{c}$ being pre-landslide mean rSSC and calving flux, respectively.

Maximum relative frontal position change (f_{MAX}) is given by:

$$f_{MAX} = max(f - f_{10/2015})$$

With f being the frontal position at a given date and $f_{10/2015}$ being the frontal position in October 2015.

References cited:

Blatter, H. (1995). Velocity and stress fields in grounded glaciers: A simple algorithm for including deviatoric stress gradients. Journal of Glaciology, 41(138), 333-344. doi:10.3189/S002214300001621X

Carrivick, J.L., Davies, B.J., James, W.H.M., Quincey, D.J., and Glasser, N.F., 2016, Distributed ice thickness and glacier volume in southern South America: Global and Planetary Change, v. 146, p. 122–132, doi:10.1016/j.gloplacha.2016.09.010.

Friedl, P., Seehaus, T., & Braun, M. (2021). Global time series and temporal mosaics of glacier surface velocities, derived from Sentinel-1 data. Earth System Science Data Discussions, 1-33.

Gilbert, J.C., and Lemaréchal, C., 1989, Some numerical experiments with variable-storage quasi-Newton algorithms: Mathematical Programming, v. 45, p. 407–435, doi:10.1007/BF01589113.

Larour, E., Seroussi, H., Morlighem, M., and Rignot, E., 2012, Continental scale, high order, high spatial resolution, ice sheet modeling using the Ice Sheet System Model (ISSM): Journal of Geophysical Research: Earth Surface, v. 117, doi:10.1029/2011JF002140.

Millan, R. et al., 2019, Ice thickness and bed elevation of the Northern and Southern Patagonian Icefields: Geophysical Research Letters, p. 2019GL082485, doi:10.1029/2019GL082485.

Morlighem, M., Seroussi, H., Larour, E., and Rignot, E., 2013, Inversion of basal friction in Antarctica using exact and incomplete adjoints of a higher-order model: Journal of Geophysical Research: Earth Surface, v. 118, p. 1746–1753, doi:10.1002/jgrf.20125.

Pattyn, F. (2003), A new three-dimensional higher-order thermomechanical ice sheet model: Basic sensitivity, ice stream development, and ice flow across subglacial lakes, J. Geophys. Res., 108, 2382, doi:10.1029/2002JB002329, B8.